IEEE Access
Multidisciplinary | Rapid Review | Open Access Journal

Received September 10, 2020, accepted September 14, 2020, date of publication September 18, 2020,
date of current version October 1, 2020.

Digital Object Identifier 10.1109/ACCESS.2020.3024859

A Compact Flexible Frequency Reconfigurable Antenna for Heterogeneous Applications

NIAMAT HUSSAIN[1], (Graduate Student Member, IEEE), WAHAJ ABBAS AWAN[2], (Student Member, IEEE), SYEDA IFFAT NAQVI[3], (Member, IEEE), ADNAN GHAFFAR[4], (Student Member, IEEE), ABIR ZAIDI[5], SYED AFTAB NAQVI[6], ADNAN IFTIKHAR[7], (Member, IEEE), AND XUE JUN LI[4], (Senior Member, IEEE)

[1]Department of Computer and Communication Engineering, Chungbuk National University, Cheongju 28644, South Korea
[2]Department of Integrated IT Engineering, Seoul National University of Science and Technology, Seoul 01811, South Korea
[3]Telecommunication Engineering Department, University of Engineering and Technology, Taxila 47080, Pakistan
[4]Department of Electrical and Electronic Engineering, Auckland University of Technology, Auckland 1010, New Zealand
[5]Laboratory EEA & TI, Department of Electrical Engineering, Hassan II University, Casablanca 20000, Morocco
[6]Department of Electrical and Computer Engineering, COMSATS University Islamabad, Sahiwal 57000, Pakistan
[7]Department of Electrical and Computer Engineering, COMSATS University Islamabad, Islamabad 45550, Pakistan

Corresponding authors: Syeda Iffat Naqvi (iffat.naqvi@uettaxila.edu.pk) and Syed Aftab Naqvi (aftabnaqvi@cuisahiwal.edu.pk)

ABSTRACT This paper presents a compact frequency reconfigurable antenna for flexible devices and conformal surfaces. The antenna consists of a simple easy to fabricate structure consisting of a stub loaded circular radiator, designed on commercially available RT5880 flexible substrate ($\varepsilon_r = 2.2$) with a thickness of 0.254 mm. The combination of stub loading and slot etching techniques are utilized to achieve the advantages of compactness, frequency reconfigurability, wide impedance bandwidth, and stable radiation pattern with structural conformability. The frequency reconfigurability is achieved by employing two p-i-n diodes. Simulated and experimental results showed that the antenna operates in various important commercial bands, such as S-band (2 GHz– 4 GHz), Wi-Max (3.5 GHz and 5.8 GHz), Wi-Fi (3.6 GHz, 5 GHz, and 5.9 GHz), 5G sub-6-GHz (3.5 GHz and 4.4 GHz – 5 GHz), and ITU-band (7.725 GHz – 8.5 GHz) with the additional advantages of structural conformability. Furthermore, the performance comparison of the proposed flexible antenna with the state-of-the-art flexible antennas in terms of compactness, frequency reconfigurability, and number of operating bands demonstrates the novelty of the proposed antenna and its potential application in heterogeneous applications.

INDEX TERMS CPW-fed, conformability, frequency reconfigurable, heterogeneous applications, miniaturized, multiband, portable, wideband.

I. INTRODUCTION

Recently, the world has witnessed a rapid revolution in the wireless communication industry due to the pressing demand to reach more users while maintaining a reliable communication system meeting the end-user requirements. As a result, a series of modern applications and standards have emerged including fifth generation (5G) of communication, internet of things (IoT), big data applications, and vehicular communications, etc. [1]. However, these emerging technologies are posing new challenges with respect to radio spectrum congestion and have overlapped allocation of wireless frequency bands. The phenomenon of antenna reconfigurability for its promising characteristic of tuning the operating frequency for the desired applications has made its marks to handle such challenges [2].

On the other hand, flexible electronic technology is classified among the most interesting research area in today's world due to the rapid increase in demand of flexible wireless electronic devices like wearables, vehicles sensors, and conformal structure etc. [3]. Moreover, the flexible antennas have over-performance compared to rigid devices, in terms of compactness, flexibility, durability, lightweight, and energy efficiency [4]. However, the antenna designers working on flexible antennas must address some challenges, including the shift of the resonant frequency and degradation impedance mismatch due to the variation of effective capacitance during bending of the antenna [5]. In addition,

The associate editor coordinating the review of this manuscript and approving it for publication was Davide Comite.

the proximity of the antenna to human tissue imposes other constraints such as gain reduction and the disruption of the antenna impedance matching [6], [7].

Other than the reconfiguration and flexibility characteristics, the antenna compactness is highly appreciated as the miniaturized antennas significantly reduce the size of electronic systems [8]. Therefore, the combination of flexibility with compactness makes the antennas preferable for modern communication systems and devices [9]. Several low-profile, compact single-band, multi-band reconfigurable antennas [10], [11], and UWB flexible antennas are reported in the literature [12]–[20]. However, modern flexible devices demand operation at multiple frequency bands, robust band switching, and compactness in a single antenna [21]. Thus, the applications of the above-mentioned antennas may become limited.

In [21], [22], CPW fed quad-band and penta-band antennas were reported. The work proposed in [21] shows the compact size and more bands as compared to reported work in [22], however, the use of copper tape instead of practical diodes do not provide efficient results and limits their application for practical applications. Another CPW fed tri-band antenna is presented in [23]. Although the results reported were in good agreement with simulations, however, the antenna presents a larger size along with an insufficient number of operating bands. On the other hand, the reported work in [24] has the advantage of multimode functionality i.e. wideband mode and two dual-band modes, but the working frequency range of the antenna is from 2 GHz to 4 GHz, which is not suitable for UWB applications. In [25], a high gain dual band frequency reconfigurable antenna is presented. The high gain is achieved by compromising on antenna size, which limits its application for compact devices.

Another interesting work is reported in [26], where researchers used two varactor diodes to achieve continuous frequency reconfigurability. Besides the disadvantage of narrowband and larger dimensions, it also has the disadvantage of high cost due to newly developed material. In [27], a monopole antenna is presented where the main radiator is connected with an L-shaped and U-shaped radiator using p-i-n diode. Depending upon the state of the diode, the antenna can resonate in single-band or dual-band operating mode. Although the antenna is compact but still the working frequency range is not suitable for many applications including UWB applications. To sum up the above discussion: A lot of work on the flexible and reconfigurable antennas has been done. However, the design of a single antenna having the advantages of maximum operating bands, wide operating frequency range, and a high level of compactness is still a challenge for researchers working in the area of flexible antennas.

In this paper, a compact, flexible, and multi-band CPW-fed slotted circular patch antenna is presented. The antenna is loaded with a rectangular stub for bandwidth enhancement. Two slots are etched on the circular radiator structure to achieve a multi-mode and multi-band behavior with the help of two p-i-n diodes. The presented antenna operates in dual-band and tri-band mode by varying the basing state of the two diodes. The major contribution of this work can be some up as:

- The presented antenna offers significant compactness with the additional advantages of multiband mode and frequency reconfigurability as compared to the state-of-the-art works.
- To the best of authors' knowledge, this is the first antenna of its kind operating at a wide frequency band ranging 2.05 – 10.7 GHz.
- Besides a moderate gain, wide bandwidth, and low return loss characteristics, the antenna also exhibits consistent results in both rigid and bending conditions. This makes the antenna suitable for modern flexible devices like wearables, vehicle sensors, etc.

The rest of the paper is organized as follows. The design methodology of the antenna is described in Section II. The comparison of the simulated and measured results is presented in Section III along with a brief comparison with the most recent works reported in the literature. Finally, the article is concluded in Section IV.

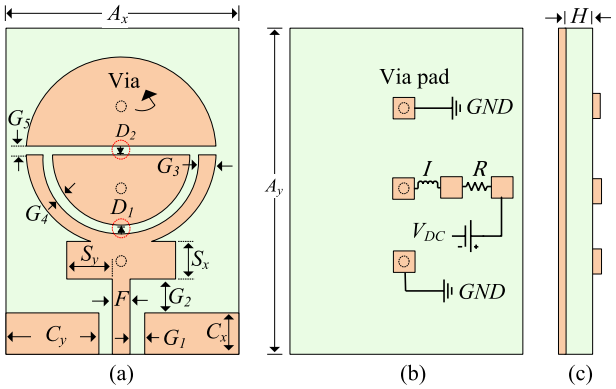

FIGURE 1. Schematic of the proposed antenna (a) top-view (b) bottom view showing the incorporation of pads for biasing circuitry, and (c) side-view.

II. THEORY AND DESIGN METHODOLOGY OF THE PROPOSED ANTENNA

The schematic of the proposed frequency reconfigurable antenna is shown in Fig. 1 (a-c). The antenna is etched on top side of a thin ROGERS RT5880LZ substrate having thickness (h) = 0.254 mm, relative permittivity (ε_r) = 2.1 and dissipation constant ($tan\ \delta$) = 0.002. Thin substrates are famous to design compact microwave circuity due to the tightly bound fields at the cost of relatively narrow bandwidth [28]. Coplanar waveguide (CPW) feeding technique as compared to other feeding techniques create extra modes and has less quality factor (Q), thus results in wide and multiband resonances [29]–[34]. Therefore, in this work, CPW feed is used to excite the radiating circular patch to achieve multi-

band resonance in proposed slotted circular patch antenna [35].

The resonating frequency f_o of the overall circular radiator is calculated by using equation given in [36]:

$$f_o = \frac{1.8412 \times c}{4\pi R_{req}\sqrt{\varepsilon_r}} \tag{1}$$

where c is the speed of the light and R_{req} is the effective radius of the circular patch which is calculated using:

$$R_{req} = R_o\sqrt{1 + \frac{2H}{\pi\varepsilon_r R_o(ln(\frac{\pi R_o}{2H}) + 1.7726)}} \tag{2}$$

where H is the thickness of the substrate, R_o is the radius of the monopole, and ε_r is the relative permittivity of the substrate. For 5.4 GHz resonating frequency, the optimized value of $R_o = 11$ mm is obtained. Next, the rectangular stub having dimension $S_x \times S_y$ is placed between the feed line and the circular radiator to enhance the narrow bandwidth of the antenna. The enhancement in the bandwidth is observed due to the introduction of extra reactive load by the stub which significantly improved matching between feedline and radiator over wide bandwidth [8]. The impedance bandwidth ($|S_{11}| < -10$ dB) of the conventional antenna is found to be 350 MHz (2.25 GHz – 2.6 GHz) which corresponds to a fractional bandwidth of 14.6 %. Whereas the insertion of rectangular stub resulted in two passbands of 2.48 GHz – 3.28 GHz and 4.94 GHz – 9.58 GHz, as depicted in Fig. 2.

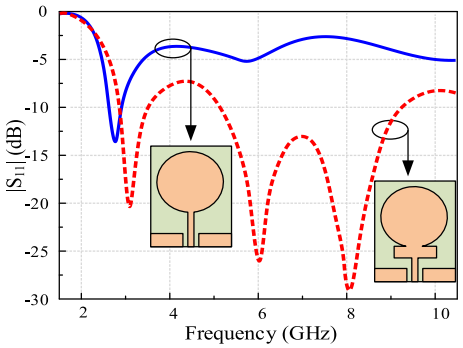

FIGURE 2. Scattering parameter ($|S_{11}|$ (dB)) comparison among conventional narrowband antenna and wideband antenna with a single notch band due to rectangular stub.

Subsequently, a semicircular slot having an internal gap of G_4 is inserted in the radiator. The insertion of this slot resulted in the mitigation of a wide band spectrum (2.9–7.7 GHz) from the operating region. The inner radius R_{in} of this slot is calculated using the relation:

$$R_{in} \approx L_{slot}/\pi, \tag{3}$$

where L_{slot} is the effective length of the slot which is numerically calculated by the following equation given in [37]:

$$L_{slot} = \frac{c}{2fr\sqrt{\varepsilon_{eff}}} \tag{4}$$

where f_r is the central frequency and $\varepsilon_{eff} \approx \frac{\varepsilon_r+1}{2}$. For the presented case, the f_r is chosen to be 5.2 GHz and the simulated optimized value of $R_{in} = 8$ mm is achieved. The gap G_4 is responsible for controlling the bandwidth of the notched frequency and it could be adjusted as per requirements of the system. Wider the gap, the wider will be the notch band region. However, 1 mm inner gap is selected for the present scenario which is equal to the physical dimension of the RF p-i-n diode (model # SMP-1345 (SC-79)). Next, a rectangular slot is etched on the radiator to add additional capacitive effects in the antenna, which resulted in the improvement of impedance matching ranging from 3.28 GHz – 4.94 GHz. Thus, a UWB antenna having an impedance bandwidth of 6.39 GHz (2.91 GHz – 9.3 GHz) is designed. The width of the rectangular slot is chosen to be 1mm as well, for the placement of the diode. The effects of the semicircular and rectangular slots, in terms of S-parameter are compared in Fig. 3.

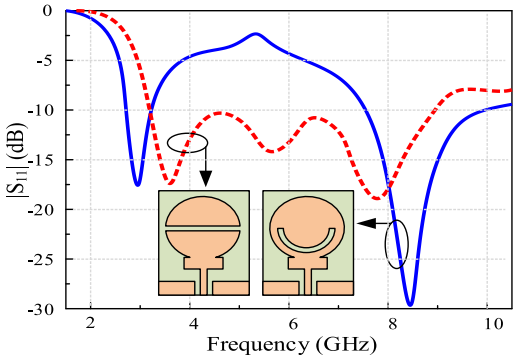

FIGURE 3. S-parameters ($|S_{11}|$ (dB)) comparison among various antenna topologies.

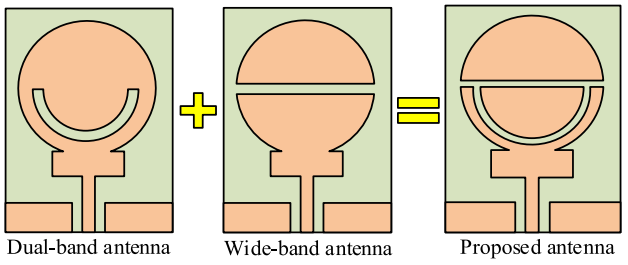

FIGURE 4. Various steps involved in the antenna designing.

Finally, both dual-band and wide-band antennas are integrated to form a single multi-band antenna. The evolution of the proposed antenna providing capability of dual- and wide-band responses is shown in Fig. 4. Afterword, two p-i-n diodes, D_1 and D_2 are deployed in the slots of the circular patch to connect and disconnect the different parts with feeding structure to get multi-mode characteristics. Commercially available finite element method based High-Frequency Structure Simulator (HFSS) is used to simulate the proposed antenna. The optimized antenna parameters obtained after

design methodology explained above are: $A_x = 35$ mm, $A_y = 25$ mm, $C_x = 5$ mm, $C_y = 11$ mm, $S_x = 5.8$ mm, $S_y = 3.85$ mm, $H = 0.254$ mm, $F = 1.8$ mm, $G_1 = 2$ mm, $G_2 = 1$ mm, $G_3 = 0.6$ mm, $G_4 = 1$ mm, and $G_5 = 1$ mm.

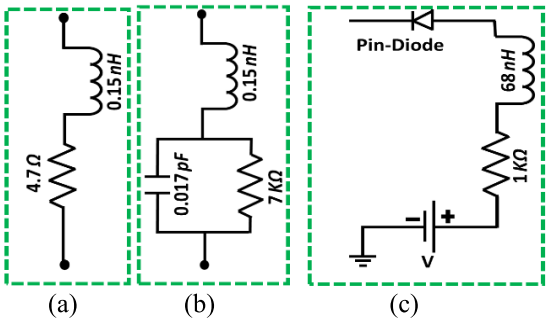

FIGURE 5. Equivalent model of diode for (a) switch ON state (b) switch OFF state (c) detailed biasing circuit.

In simulation environment, parallel lumped RLC model with values of R, L, and C shown in Figure 5 (a–b) are used to mimic diodes ON and OFF states. In addition, via and padding on the back sides of the proposed antenna as shown in Figure 1 (b) are also modeled in the simulation environment to achieve consistent simulation and measurement results. It can be seen from Figure 5 (a) that in ON state, equivalent circuit having a series combination of 4.7 Ω resistor and 0.15 *nH* inductor is modeled using parallel RLC boundary conditions. On the other hand, in OFF state, a series combination of 0.15 *nH* with a parallel combination of 7 *K*Ω resistor and 0.017 *pF* capacitor, as depicted in Figure 5(b) is modeled using RLC boundary conditions.

The utilization of ON and OFF states of p-i-n didoes change the electrical length of the radiator to allow the appropriate flow of current density. The ON and OFF states of p-i-n diodes consequently matched the impedance at different frequency bands at a time and resulted in frequency reconfigurability at multiband depending upon the RF current flowing in the resonating structures.

III. SIMULATED AND EXPERIMENTAL RESULTS

A. MEASUREMENT SETUP

To verify the simulated results, a prototype of the simulated antenna with optimized dimensions shown in Fig. 1 is fabricated and tested. A commercially available 50 Ω SMA connector is utilized to feed the antenna and Skyworks p-i-n diodes having model # SMP-1345 (SC-79) are soldered to connect three different conducting patches of the radiator.

To provide biased voltage for p-i-n diode operation, extra paddings as shown in Fig. 1 (b) and modeled in simulation environment are also etched on the bottom side of substrate. A photograph of the fabricated prototype with pads and via connection is shown in Fig. 6 (a). In particular, on the back side of the proposed antenna, the upper and lower end of the circular radiator is connected to ground through conducting via. A stable voltage V_{DC} is provided to the middle part of the radiator via the V_{DC} pad connected to the biasing circuitry

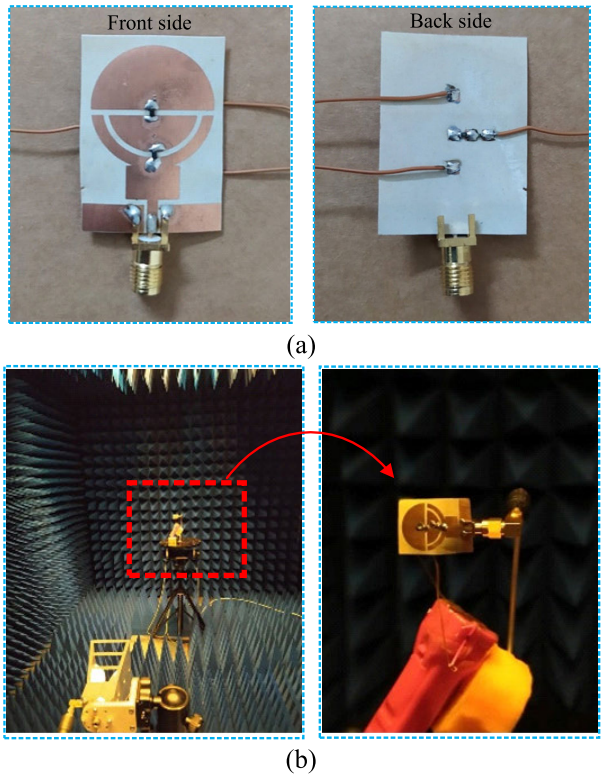

FIGURE 6. Photographs of the (a) fabricated prototype of the proposed antenna and (b) measurement setup for the farfield measurements.

of the diodes. A detailed description of the biasing circuit is shown in Fig. 5 (c). Fig. 5 (c) presents the configuration of biasing circuit where 1 KΩ resistor is used to limit the amount of DC current coming from source $V_{DC} = 3$ V, while 68 *nH* blocks the unnecessary flow of RF current towards diode. The inductor selected was low profile chip inductor 0402CT (1005), part number: 0402CT – 12NX-RW. The inductor behaved as RF choke, while thin copper wires connected the antenna biasing structure with a 3V battery, as shown in Figure 6 (a). For $|S_{11}|$ (dB) measurements, calibrated Vector Network Analyzer (VNA) is utilized, whereas broadband standard horn antenna is used for far-field measurements inside fully calibrated anechoic chamber, as depicted in Figure 6 (b).

B. SCATTERING PARAMETERS

Fig. 7 (a–c) illustrates the comparison between simulated and measured $|S_{11}|$ (dB) results. For the ease of understanding, the ON state of the diode is represented by '1' while diode in OFF state is represented by '0'. The three possible combinations of diodes are used; case-00, case-10, and case-11, where first and second digit shows the switching state of D_1 and D_2, respectively. The antenna exhibits three passbands for case-10, while dual passbands are observed for case-00 and case-11. Figure 7 (a) shows that for case-00, the simulated impedance bandwidth for the two operating bands is 3.06 GHz– 6.17 GHz and 7.1 GHz – 8.95 GHz,

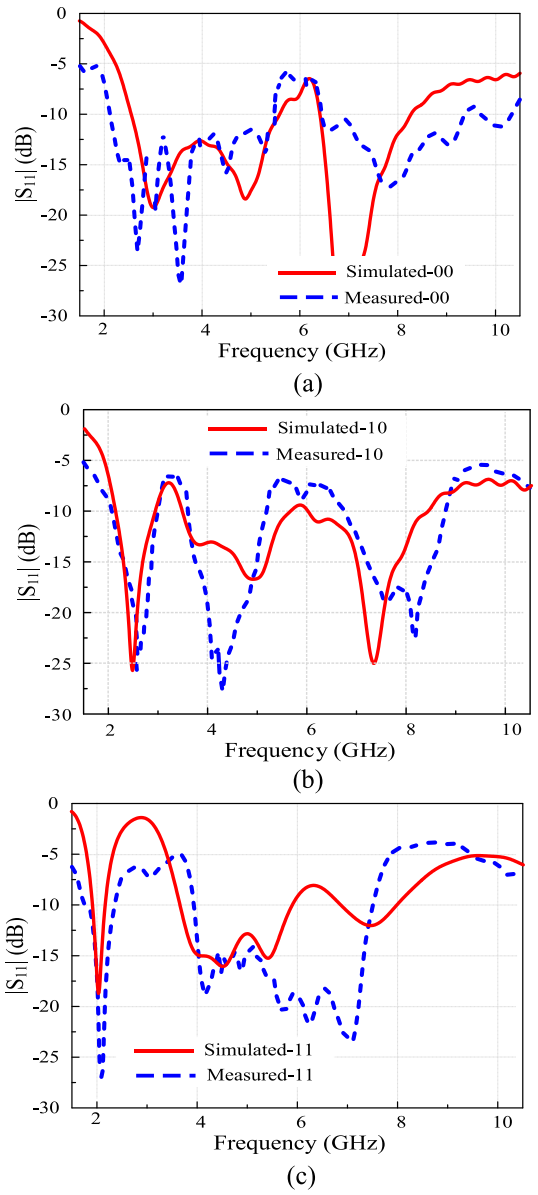

FIGURE 7. $|S_{11}|$ (dB) comparison of the proposed antenna for various diode states (a) case-00 (b) case-10 (c) case-11.

while measured values for case-00 are found to be 2.52 GHz – 6.02 GHz and 7.1 GHz – 10.7 GHz. Similarly, Fig. 7 (b) depicts the results for case-10. The three operating bands achieved in simulations are from 2.77 GHz – 3.6 GHz, 4.28 GHz – 5.98 GHz, and 7.1 – 8.9 GHz. However, 2.82 GHz – 3.56 GHz, 4.32 GHz – 5.91 GHz, and 7.4 GHz – 9.4 GHz bands are achieved in measurements.

Contrarily, dual-band response is achieved for case-11. In simulations, the impedance bandwidth of the dual-band is from 2.05 GHz – 2.36 GHz and 3.87 – 8.3 GHz, as shown in Figure 8 (c). Whereas a slight variation in impedance bandwidth of the is observed i.e. 1.98 GHz – 2.51 GHz and 3.97 GHz – 7.87 GHz, as illustrated in Fig. 7 (c). The slight difference between simulated and measured results shown in Figure 7 (a – c) is attributed to the change in inductance because of fabrication imperfections, soldering, vias platting, and connector losses.

C. SURFACE CURRENT DISTRIBUTION

To provide a better understanding of the multiband behavior of the proposed antenna using various p-i-n diodes states, the surface current density for different switching states at various frequencies are presented in Fig. 8. For OFF state of both diodes D_1 and D_2 referred as case-00, the current density is maximum across feedline, rectangular stub, and semi-circular portion, as shown Fig. 8 (a) and (b). This results in broad bandwidth around 3.5 GHz because of current density in rectangular stub and semi-circular patch, whereas other resonance at around 8 GHz is attributed to rectangular stub which corresponds to lower electrical length. Results of $|S_{11}|$ (dB) shown in Fig. 7 (a) confirm the dual-band operation when both diodes are switched OFF (case-00). For case-10 (when diode D_1 is ON and D_2 is OFF), the surface current is distributed across rectangular stub attached with semi-circular stub and middle semi-circular patch, as depicted in Fig. 8 (b-d). The mutual coupling effect and flow of RF current because of the D_1 ON state, three resonances at 3.1 GHz, 5.2 GHz, and 9 GHz are achieved. 5.2 GHz and 9 GHz resonances are because of the lower portion directly connected to feed, whereas third resonance i.e. 3.1 GHz is due to middle semi-circular patch and lower patch portion. Similarly, for case-11, when both diodes are in ON state, all the patches are connected which results in larger electrical length and showed resonance at 2.1 GHz, However, resonance at 6 GHz is achieved due to the lower portion and mutual coupling effect of the middle and higher patches. A wider bandwidth at 6 GHz is attributed to the maximum current in the rectangular stub, as shown in Fig. 8 (g). It can be concluded that by switching the states of p-i-n diodes, the change in surface current distribution results in multiband and multimode antenna (dual band and tri band modes).

D. CONFORMABILITY ANALYSIS

The proper functionality of the antenna and performance consistency under the conformability condition is one of the key requirements for the flexible antennas. Therefore, the proposed antenna is tested under conformal conditions. Next, in the simulation, the antenna is bent in the X-axis and Y-axis on a cylinder having radius (R) 25 mm. A 25 mm radius is chosen by keeping in mind that the corner of the antenna did not touch each other. For measurement purposes, the proposed antenna is bent along a cylindrical shaped Styrofoam having a radius of 25 mm, as depicted in Figure 9 (a–b).

Figure 10 (a-c) presents the comparison among simulated and measured results of magnitude of reflection coefficient $|S_{11}|$ (dB) under conformability condition. Figure 10 (a) depicts the results for case-00 where the simulated results remained same as of unbent antenna while measured results show that antenna covers additional low band region. For

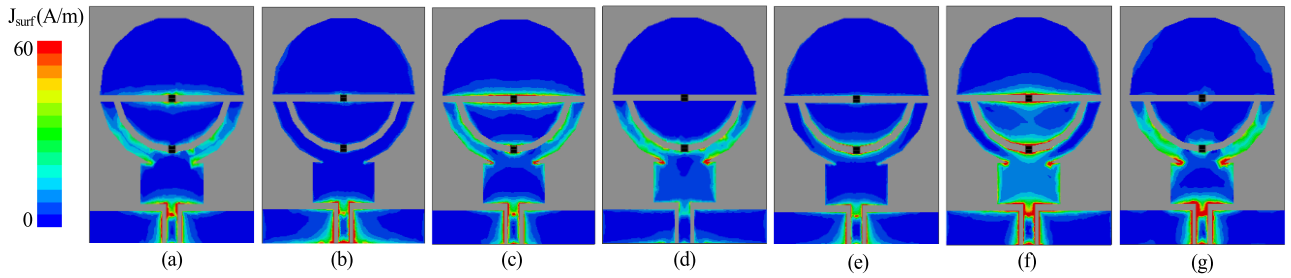

FIGURE 8. Current Desnity of proposed antenna at various frequencies. Case-00 (a) 3.5 GHz (b) 8.5 GHz; Case-10 (c) 3.1 GHz (d) 5.2 GHz (e) 9 GHz; Case-11 (f) 2.1 GHz (g) 6GHz.

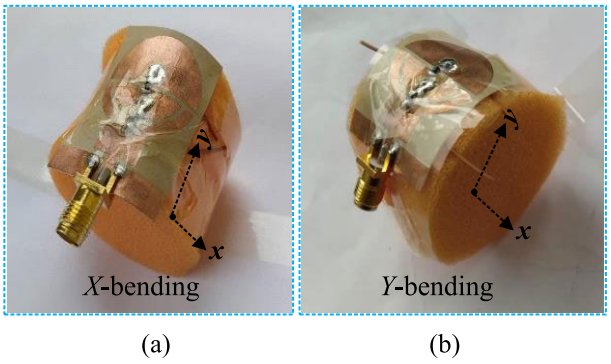

FIGURE 9. A photograph of the proposed antenna conformed on a clydrical styrofoam peformance analysis (a) bending along the *X*-axis (b) bending along the *Y*-axis.

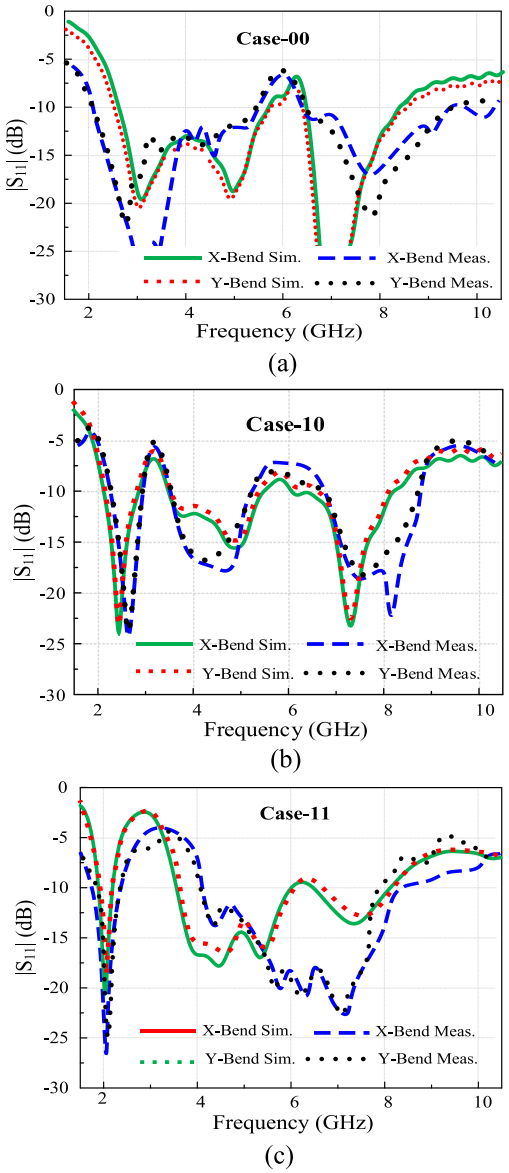

FIGURE 10. Conformability analysis comparison of the proposed antennana for various diode states (a) case-00 (b) case-10 (c) case-11.

case-10, the antenna exhibits similar results as that of unbending condition. A small and acceptable discrepancy was observed for higher bands, as illustrated in Figure 10 (b). Similarly, Figure 10 (c) presents the results for case-11. It can be observed from Figure 10 (c) that the measured results under conformability condition are in good agreement with that of the antenna under unbent condition. A small discrepancy among simulated and measured results due to imperfections in attachment of antenna with the cylindrical Styrofoam for the conformability analysis.

E. FAR-FIELD ANALYSIS

To demonstrate far-field performance of the proposed antenna, far-field radiation pattern and gain were evaluated using electromagnetic simulator and measurements. However, for brevity, the numerically selected frequencies for case-00 at 3.5 GHz and 8.5 GHz where antenna exhibits nearly omni-directional radiation pattern in principal H-plane ($\theta = 90°$) while a bidirectional radiation pattern is observed for E-plane ($\theta = 0°$), as depicted in Fig.11 (a–b). The simulated value of gain is observed 3.21 dBi and 5.23 dBi while 3.17 dBi and 5.21 dBi measured gain at 3.5 GHz and 8.5 GHz, respectively was achieved. Likewise, for case-10, the radiation patterns at 3.1 GHz, 5.2 GHz, and 9 GHz are measured. It is observed that antenna exhibits omnidirectional radiation pattern in *H*-plane while a slightly tilted bidirectional radiation pattern is observed for *E*-plane for all selected frequencies, as illustrated in Fig. 11 (c - e).

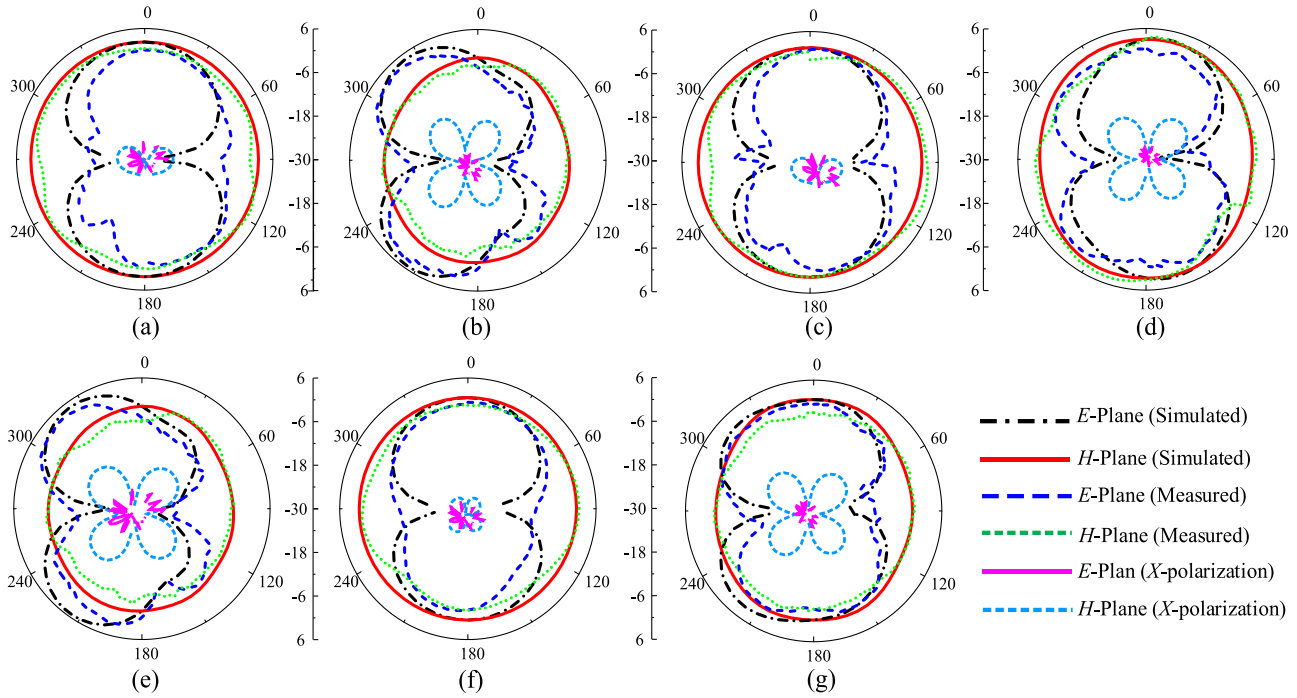

FIGURE 11. Comparison between simulated and measured radiation pattern. Case-00 (a) 3.5 GHz (b) 8.5 GHz; Case-10 (c) 3.1 GHz (d) 5.2 GHz (e) 9 GHz; Case-11 (f) 2.1 GHz (g) 6GHz.

TABLE 1. Comparison of simulated and measured results of the proposed antenna.

Switching Case	Simulated B.W (GHz)	Measured B.W (GHz)	Simulated Gain (dB)	Measured Gain (dB)	Simulated Efficiency (%)	Measured Efficiency (%)
00	3.06–6.17	2.52–6.02	3.21	3.17	89	87.3
	7.1–8.95	7.1–10.7	5.23	5.21	86.4	85.9
10	2.77–3.6	2.82–3.56	2.76	2.7	85.1	84.7
	4.28–5.98	4.32–5.91	4.7	4.71	87	86.2
	7.1–8.9	7.4–9.4	5.44	5.31	84.4	83.5
11	2.05–2.36	1.98–2.51	2.1	2.02	78	77.4
	3.87–8.3	3.97–7.87	5.28	5.2	85.5	84.7

The simulated gain value at selected frequency of 3.1 GHz, 5.2 GHz and 9 GHz are 2.76 dBi, 4.7 dBi, and 5.44 dBi, respectively. However, measured gain values of 2.7 dBi @ 3.1 GHz, 4.71 dBi @ 5.2 GHz, and 5.31 dBi @ 9 GHz are observed. Similarly, for case-11, frequencies of 2.1 GHz and 6 GHz are selected. Likewise, previous cases, the antenna exhibits omni-directional radiation pattern and bidirectional radiation pattern in principal H-plane ($\theta = 90°$) and E-plane ($\theta = 0°$), respectively. Moreover, the simulated gain value of 2.1 dBi and 5.28 dBi while measured gain value of 2.02 dBi and 5.2 dBi at 2.1 GHz, and 7 GHz, respectively is achieved. It can be observed that at higher frequencies (8 GHz and 9 GHz), the radiation pattern is little deteriorated since the equivalent radiating area increased at high frequencies. Moreover, for all selected frequencies for various switching cases, the antenna exhibits minimum cross polarization of less than −10dB, as depicted in Figure 11 (a–e). Overall, a fair agreement between simulated and measured results is observed. Table 1 presents the summary of the simulated and measured results of the proposed antenna.

F. PERFORMANCE COMPARISON

Table 2 presents a brief comparison of the proposed antenna with recently reported antennas for similar applications. The presented work outperforms the competitor works in terms of electrical size (with respect to lowest resonance) by showing at least 40.74% miniaturization and the total number of operating bands are seven. Besides this, the presented antenna covers the widest band ranging from 1.98 GHz to 10.7 GHz while the rest of the reported designs demonstrate antennas frequency reconfigurability within a close range. Moreover, good agreement between simulated and measured results in both conformal and non-conformal cases made this proposed antenna a potential candidate for heterogeneous applications possessing multiband antennas in modern flexible devices.

TABLE 2. Performance comparison of the proposed antenna with state-of-the-art works.

Refs.	Antenna Size (λ_0^2)	Operational Mode	-10 dB $\lvert S_{11}\rvert$ BW (GHz)	Reconfigurability Technique
[21]	0.27×0.23	Tri-band	4.19–4.48, 5.98–6.4 & 6.8–7 / 3.42–4, 5.4–5.68 & 6.8–7	Copper Tape
[22]	0.39×0.37	Dual band	3.9–4.53 & 7.2–7.8	Copper Tape
		Single band	4.7–5.4 / 3.9–4.6 / 5–6	
[23]	0.45×0.23	Single band	2.34–2.5	PIN Diode
		Dual band	2.27–2.45 & 3.5–3.77	
[24]	0.36×0.24	Wideband	2.18–3.52	PIN Diode
		Dual band	2.16–3.19 & 3.55–3.795 / 2.15–2.77 & 3.07–3.42	
[25]	0.69×0.65	Single band	2.4–2.5	PIN Diode
		Dual band	2.35–2.52 & 3.28–3.38	
[26]	0.46×0.46	Single band	2.3–2.68 (BW*) / 2.26–3.9	Varactors
[27]	1.0×0.97	Single band	1.65–2.5 & 2.8–3.39 / 1.56–1.79 & 2.5–3.17 / 2.28–2.72	PIN Diode
		Dual band	3.1–3.8	
This Work	**0.23×0.16**	**Dual band**	**2.52–6.02 & 7.1–10.7 / 1.98–2.51 & 3.97–7.87**	**PIN Diode**
		Tri-band	**2.82–3.56, 4.32–5.91 & 7.4–9.4**	

λ_0 is free space wavelength at lowest resonating frequency, *BW stands for bandwidth, BW* represent the total bandwidth covered by varactors diode*

IV. CONCLUSION

A miniaturized frequency reconfigurable flexible antenna operating at multiple on demand frequency mode is presented in this paper. Rectangular stub, semicircular, and rectangular slot are deployed as radiating parts to attain wideband and multiband operation. Two p-i-n diodes are used to connect the radiating parts of the antenna to resonate at different frequency bands. These sets of frequencies are achieved corresponding connection and disconnection of the radiating patch by using configuration of the p-i-n diodes. A dual band operation for case-00, tri band for case-10 and dual band for case-11 is achieved. The presented antenna attains at least 40.74% miniaturization in size and operates in more bands as compared to the most recent work reported in the literature. Moreover, a good agreement between simulated and measured results for both conformal and non-conformal scenarios make the proposed antenna a potential candidate for the devices operating in multiple allocated spectrum of S-band, Wi-Max, Wi-Fi, 5G sub-6-GHz, and ITU-band.

REFERENCES

[1] T. Li, Y. Dong, P. Fan, and K. B. Letaief, "Wireless communications with RF-based energy harvesting: From information theory to green systems," *IEEE Access*, vol. 5, pp. 27538–27550, 2017.

[2] Y. J. Guo, P.-Y. Qin, S.-L. Chen, W. Lin, and R. W. Ziolkowski, "Advances in reconfigurable antenna systems facilitated by innovative technologies," *IEEE Access*, vol. 6, pp. 5780–5794, 2018.

[3] A. Zaidi, W. A. Awan, N. Hussain, and A. Baghdad, "A wide and tri-band flexible antennas with independently controllable notch bands for sub-6-GHz communication system," *Radioengineering*, vol. 29, no. 1, pp. 44–51, Apr. 2020.

[4] H. Khaleel, Ed, *Innovation in Wearable and Flexible Antennas*. Boston, MA, USA: Wit Press, 2014.

[5] W. A. Awan, N. Hussain, and T. T. Le, "Ultra-thin flexible fractal antenna for 2.45 GHz application with wideband harmonic rejection," *AEU-Int. J. Electron Commun.*, vol. 110, Oct. 2019, Art. no. 152851.

[6] A. Smida, A. Iqbal, A. J. Alazemi, M. I. Waly, R. Ghayoula, and S. Kim, "Wideband wearable antenna for biomedical telemetry applications," *IEEE Access*, vol. 8, pp. 15687–15694, 2020.

[7] A. Iqbal, A. J. Alazemi, and N. Khaddaj Mallat, "Slot-DRA-based independent dual-band hybrid antenna for wearable biomedical devices," *IEEE Access*, vol. 7, pp. 184029–184037, 2019.

[8] W. A. Awan, A. Zaidi, N. Hussain, A. Iqbal, and A. Baghdad, "Stub loaded, low profile UWB antenna with independently controllable notch-bands," *Microw. Opt. Technol. Lett.*, vol. 61, pp. 2447–2454, Nov. 2019.

[9] F. Faisal, Y. Amin, Y. Cho, and H. Yoo, "Compact and flexible novel wideband flower-shaped CPW-fed antennas for high data wireless applications," *IEEE Trans. Antennas Propag.*, vol. 67, no. 6, pp. 4184–4188, Jun. 2019.

[10] A. Iftikhar, S. M. Asif, J. M. Parrow, J. W. Allen, M. S. Allen, A. Fida, and B. D. Braaten, "Changing the operation of small geometrically complex EBG-based antennas with micron-sized particles that respond to magnetostatic fields," *IEEE Access*, vol. 8, pp. 78956–78964, 2020.

[11] A. Iftikhar, J. Parrow, S. Asif, A. Fida, J. Allen, M. Allen, B. Braaten, and D. Anagnostou, "Characterization of novel structures consisting of micron-sized conductive particles that respond to static magnetic field lines for 4G/5G (Sub-6 GHz) reconfigurable antennas," *Electronics*, vol. 9, no. 6, p. 903, May 2020.

[12] Q. H. Abbasi, M. U. Rehman, X. Yang, A. Alomainy, K. Qaraqe, and E. Serpedin, "Ultrawideband band-notched flexible antenna for wearable applications," *IEEE Antennas Wireless Propag. Lett.*, vol. 12, pp. 1606–1609, 2013.

[13] K. W. Lui, O. H. Murphy, and C. Toumazou, "A wearable wideband circularly polarized textile antenna for effective power transmission on a wirelessly-powered sensor platform," *IEEE Trans. Antennas Propag.*, vol. 61, no. 7, pp. 3873–3876, Jul. 2013.

[14] A. Arif, M. Zubair, M. Ali, M. U. Khan, and M. Q. Mehmood, "A compact, low-profile fractal antenna for wearable on-body WBAN applications," *IEEE Antennas Wireless Propag. Lett.*, vol. 18, no. 5, pp. 981–985, May 2019.

[15] B. Luadang, A. Sakonkanapong, S. Dentri, R. Pansomboon, and C. Phongcharoenpanich, "NFC-enabled far-field antenna on PET flexible substrate for 3G/4G/LTE mobile devices," *IEEE Access*, vol. 7, pp. 171966–171973, 2019.

[16] R. B. Simorangkir, A. Kiourti, and K. P. Esselle, "UWB wearable antenna with a full ground plane based on PDMS-embedded conductive fabric," *IEEE Antennas Wirel Propag Lett.*, vol. 17, no. 3, pp. 493–496, 2018.

[17] K. N. Paracha, S. K. A. Rahim, H. T. Chattha, S. S. Aljaafreh, S. U. Rehman, and Y. C. Lo, "Low-cost printed flexible antenna by using an office printer for conformal applications," *Int. J. Antennas Propag.*, vol. 2018, pp. 1–7, Feb. 2018.

[18] W. Li, Y. Hei, P. M. Grubb, X. Shi, and R. T. Chen, "Compact inkjet-printed flexible MIMO antenna for UWB applications," *IEEE Access*, vol. 6, pp. 50290–50298, 2018.

[19] B. Mohamadzade, R. B. V. B. Simorangkir, R. M. Hashmi, Y. Chao-Oger, M. Zhadobov, and R. Sauleau, "A conformal band-notched ultrawideband antenna with monopole-like radiation characteristics," *IEEE Antennas Wireless Propag. Lett.*, vol. 19, no. 1, pp. 203–207, Jan. 2020.

[20] L. I. Balderas, A. Reyna, M. A. Panduro, C. Del Rio, and A. R. Gutierrez, "Low-profile conformal UWB antenna for UAV applications," *IEEE Access*, vol. 7, pp. 127486–127494, 2019.

[21] A. Ahmad, F. Arshad, S. I. Naqvi, Y. Amin, H. Tenhunen, and J. Loo, "Flexible and compact spiral-shaped frequency reconfigurable antenna for wireless applications," *IETE J. Res.*, vol. 66, no. 1, pp. 22–29, 2018.
[22] M. U. Hassan, F. Arshad, S. I. Naqvi, Y. Amin, and H. Tenhunen, "A compact flexible and frequency reconfigurable antenna for quintuple applications," *Radioengineering*, vol. 26, no. 3, pp. 655–661, Sep. 2017.
[23] S. M. Saeed, C. A. Balanis, and C. R. Birtcher, "Inkjet-printed flexible reconfigurable antenna for conformal WLAN/WiMAX wireless devices," *IEEE Antennas Wireless Propag. Lett.*, vol. 15, pp. 1979–1982, 2016.
[24] K. Saraswat and A. R. Harish, "Flexible dual-band dual-polarised CPW-fed monopole antenna with discrete-frequency reconfigurability," *IET Microw., Antennas Propag.*, vol. 13, no. 12, pp. 2053–2060, Oct. 2019.
[25] S. M. Saeed, C. A. Balanis, C. R. Birtcher, A. C. Durgun, and H. N. Shaman, "Wearable flexible reconfigurable antenna integrated with artificial magnetic conductor," *IEEE Antennas Wireless Propag. Lett.*, vol. 16, pp. 2396–2399, 2017.
[26] R. B. V. B. Simorangkir, Y. Yang, K. P. Esselle, and B. A. Zeb, "A method to realize robust flexible electronically tunable antennas using polymer-embedded conductive fabric," *IEEE Trans. Antennas Propag.*, vol. 66, no. 1, pp. 50–58, Jan. 2018.
[27] H. F. Abutarboush and A. Shamim, "A reconfigurable inkjet-printed antenna on paper substrate for wireless applications," *IEEE Antennas Wireless Propag. Lett.*, vol. 17, no. 9, pp. 1648–1651, Sep. 2018.
[28] N. Hussain, M.-J. Jeong, J. Park, and N. Kim, "A broadband circularly polarized Fabry–Pérot resonant antenna using a single-layered PRS for 5G MIMO applications," *IEEE Access*, vol. 7, pp. 42897–42907, 2019.
[29] L. M. Si and X. Lv, "CPW-fed multi-band omni-directional planar microstrip antenna using composite metamaterial resonators for wireless communications," *Prog. Electromagn. Res.*, vol. 83, pp. 46–133, 2008.
[30] R. P. Dwivedi and U. K. Kommuri, "CPW feed dual band and wideband antennas using crescent shape and T-shape stub for Wi-Fi and WiMAX application," *Microw. Opt. Technol. Lett.*, vol. 59, no. 10, pp. 2586–2591, 2017.
[31] W.-C. Liu, C.-M. Wu, and N.-C. Chu, "A compact CPW-fed slotted patch antenna for dual-band operation," *IEEE Antennas Wireless Propag. Lett.*, vol. 9, pp. 110–113, 2010.
[32] M. J. Hua, P. Wang, S. L. Yuan, and Y. Zheng, "Compact tri-band CPW-fed antenna for WLAN/WiMAX applications," *Electron. Lett.*, vol. 49, no. 18, pp. 1118–1119, Aug. 2013.
[33] W. A. Awan, N. Hussain, S. A. Naqvi, A. Iqbal, R. Striker, D. Mitra, and B. D. Braaten, "A miniaturized wideband and multi-band on-demand reconfigurable antenna for compact and portable devices," *AEU - Int. J. Electron. Commun.*, vol. 122, Jul. 2020, Art. no. 153266.
[34] R. Z. Wu, P. Wang, Q. Zheng, and R. P. Li, "Compact CPW-fed triple-band antenna for diversity applications," *Electron Lett*, vol. 51, no. 10, pp. 735–736, 2015.
[35] Y. J. Li, Z. Y. Lu, and L. S. Yang, "CPW-fed slot antenna for medical wearable applications," *IEEE Access*, vol. 7, pp. 42107–42112, 2019.
[36] C. A. Balanis, *Advanced Engineering Electromagnetics*. Hoboken, NJ, USA: Wiley, 1999.
[37] S. I. Naqvi, A. H. Naqvi, F. Arshad, M. A. Riaz, M. A. Azam, M. S. Khan, Y. Amin, J. Loo, and H. Tenhunen, "An integrated antenna system for 4G and millimeter-wave 5G future handheld devices," *IEEE Access*, vol. 7, pp. 116555–116566, 2019.

NIAMAT HUSSAIN (Graduate Student Member, IEEE) received the B.S. degree in electronics engineering from the Dawood University of Engineering and Technology, Karachi, Pakistan, in 2014, and the M.S. degree in electrical and computer engineering from Ajou University, Suwon, South Korea. He is currently pursuing the Ph.D. degree in information and communication engineering with Chungbuk National University, Chungju-si, South Korea. His research is mainly focused on lens-coupled antennas, metasurface antennas, metamaterial antennas, UWB antennas, mmWave antennas, and terahertz antennas. He received the Best Paper Award on 2017, for his presented article at Korea Winter Conference.

WAHAJ ABBAS AWAN (Student Member, IEEE) received the B.S. degree in electrical engineering from COMSATS University Islamabad, Sahiwal Campus, in 2019. He is currently pursuing the M.S. degree in integrated IT engineering with the Seoul National University of Science and Technology, Seoul, South Korea. He is also a Research Assistant with the Electromagnetic Measurement and Application (EMMA) Laboratory, Seoul National University of Science and Technology. He is the author of more than 15 peer-reviewed conference and journal articles. His research interests include electrically small, flexible, and reconfigurable antennas.

SYEDA IFFAT NAQVI (Member, IEEE) received the B.Sc. degree in computer engineering and the M.Sc. degree in telecommunication engineering from the University of Engineering and Technology, Taxila, Pakistan, in 2006 and 2011, respectively. She is currently an Assistant Professor with the University of Engineering and Technology. Her current research interest includes the design and implementation of multiple antenna array systems for current 4G and next generation millimeter-wave 5G mobile communication applications.

ADNAN GHAFFAR (Student Member, IEEE) received the B.Sc. degree in computer engineering from BZU Multan, Pakistan, in 2010, and the M.S. degree in circuits and systems from Lanzhou Jiaotong University, Lazhou, China, in 2015. He is currently pursuing the Ph.D. degree in electrical and electronics engineering with the Auckland University of Technology, Auckland, NZ, USA. His current research interest includes RF circuits, reconfigurable antenna, embedded system, metasurface antenna, flexible, and wearable antennas.

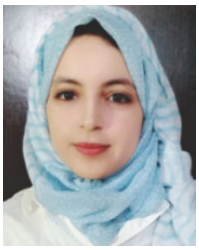

ABIR ZAIDI received the master's degree in microelectronics, telecommunication and industrial data processing from Hassan II University, Mohammedia-Casablanca, Morocco, where she is currently pursuing the Ph.D. degree with the Laboratory of Electronics, Energy, Automatics and Data Processing (EEA&TI). Her research interest includes the design of the multiband microstrip patch antennas to operate in the 5G and millimeter wave band.

SYED AFTAB NAQVI received the M.Sc. and M.Phil. degrees in electronics from Quaid-I-Azam University Islamabad, Pakistan, in 2008 and 2011, respectively, and the Ph.D. degree in electrical and computer engineering from North Dakota State University, Fargo, ND, USA, in 2014. He has been an Assistant Professor with the Department of Electrical and Computer Engineering, COMSATS University Islamabad, Sahiwal, Pakistan, since 2015. His research interests include electromagnetic cloaking, antenna design for biosensors, MIMO antenna array for 5G applications, and methods in computational electromagnetics. He was awarded with Research Productivity Award (RPA) in 2012 by the Pakistan Council for Science and Technology (PCST). He was also awarded RPA by the Commission on Science and Technology for Sustainable Development in the South (COMSATS Pakistan) in 2015, 2016, and 2017. He was listed as a Productive Scientist of Pakistan in the gazettes issued by PCST in 2015, 2016, and 2017.

ADNAN IFTIKHAR (Member, IEEE) received the B.S. degree in electrical engineering from COMSATS University Islamabad (CUI), Pakistan, in 2008, the M.S. degree in personal mobile and satellite communication from the University of Bradford, U.K., in 2010, and the Ph.D. degree in electrical and computer engineering from North Dakota State University (NDSU), USA, in 2016. He is currently an Assistant Professor with the Department of Electrical and Computer Engineering, CUI. He has authored or coauthored 30 journals and conference publications. His current research interests include applied electromagnetic, reconfigurable antennas, leaky wave antennas, phased array antennas, and energy harvesting for low power devices.

XUE JUN LI (Senior Member, IEEE) received the B.Eng. (Hons.) and Ph.D. degrees in electrical and electronic engineering from Nanyang Technological University (NTU), Singapore, in 2004 and 2008, respectively. From November 2007 to July 2008, he was as a Research Engineer and as a Research Fellow with the Network Technology Research Centre, NTU. From August 2008 to September 2008, he was a Research Scientist with the Temasek Laboratories, NTU. From September 2008 to May 2011, he was a Faculty Member with the School of Electrical and Electronic Engineering, NTU. From June 2011 to January 2013, he was a Research Scientist with the Institute for Infocomm Research (I2R), Agency for Science, Technology and Research (A*STAR), Singapore. Since January 2013, he has been a Senior Lecturer with the Department of Electrical and Electronic Engineering, School of Engineering, Auckland University of Technology (AUT). His research interests include design/analysis of wireless networking protocols, modeling/design of radio frequency integrate circuits, and system optimizations.